Biophysical Chemistry 254 (2019) 106260

Contents lists available at ScienceDirect

Biophysical Chemistry

journal homepage: www.elsevier.com/locate/biophyschem

# Structure and thermodynamics of aqueous urea solutions from ambient to kilobar pressures: From thermodynamic modeling, experiments, and first principles simulations to an accurate force field description

Christoph Hölzl[a,1], Patrick Kibies[b], Sho Imoto[c], Jan Noetzel[c], Michael Knierbein[d], Paul Salmen[e], Michael Paulus[e], Julia Nase[e], Christoph Held[d], Gabriele Sadowski[d], Dominik Marx[c], Stefan M. Kast[b], Dominik Horinek[a,*]

[a] Institut für Physikalische und Theoretische Chemie, Universität Regensburg, 93040 Regensburg, Germany
[b] Physikalische Chemie III, Technische Universität Dortmund, 44227 Dortmund, Germany
[c] Lehrstuhl für Theoretische Chemie, Ruhr-Universität Bochum, 44780 Bochum, Germany
[d] Laboratory of Thermodynamics, Technische Universität Dortmund, 44227 Dortmund, Germany
[e] Fakultät Physik/DELTA, Technische Universität Dortmund, 44221 Dortmund, Germany

## HIGHLIGHTS

- Experimental densities of urea solutions are determined up to 5 kbar.
- Aqueous urea solutions are studied by theoretical methods up to 10 kbar
- A new nonpolarizable force field for urea in aqueous solutions is developed.

## GRAPHICAL ABSTRACT

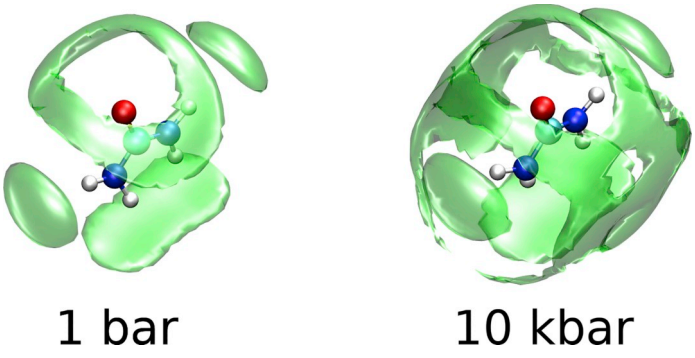


## ABSTRACT

Molecular simulations based on classical force fields are a powerful method for shedding light on the complex behavior of biomolecules in solution. When cosolutes are present in addition to water and biomolecules, subtle balances of weak intermolecular forces have to be accounted for. This imposes high demands on the quality of the underlying force fields, and therefore force field development for small cosolutes is still an active field. Here, we present the development of a new urea force field from studies of urea solutions at ambient and elevated hydrostatic pressures based on a combination of experimental and theoretical approaches. Experimental densities and solvation shell properties from ab initio molecular dynamics simulations at ambient conditions served as the target properties for the force field optimization. Since urea is present in many marine life forms, elevated hydrostatic pressure was rigorously addressed: densities at high pressure were measured by vibrating tube densitometry up to 500 bar and by X-ray absorption up to 5 kbar. Densities were determined by the perturbed-chain statistical associating fluid theory equation of state. Solvation properties were determined by embedded cluster integral equation theory and ab initio molecular dynamics. Our new force field is able to capture the properties of urea solutions at high pressures without further high-pressure adaption, unlike trimethylamine-N-oxide, for which a high-pressure adaption is necessary.

* Corresponding author.
*E-mail addresses:* stefan.kast@tu-dortmund.de (S.M. Kast), dominik.horinek@ur.de (D. Horinek).
[1] Current address: Lehrstuhl für Theoretische Chemie, Ruhr-Universität Bochum, 44780 Bochum, Germany.

https://doi.org/10.1016/j.bpc.2019.106260
Received 12 July 2019; Received in revised form 29 August 2019; Accepted 29 August 2019
Available online 03 September 2019

## 1. Introduction

Urea is abundant in biological systems. It is a product of protein metabolism, where it serves organisms as a sink for ammonia. In the presence of urea, proteins and other biopolymers face its denaturing effect, and organisms tend to expunge urea through the kidney. In this light, it is astonishing that some marine animals show significantly elevated levels of urea [1]. These organisms exist under rather extreme conditions: the surrounding sea water has a high salinity, which puts organisms under severe osmotic stress, and the hydrostatic pressure in the sea rises to levels that can destabilize proteins [2]. These detrimental effects are counterbalanced by so-called 'compatible cosolutes' or supernaturants, most prominently trimethylamine-N-oxide (TMAO), small cosolutes that stabilize folded proteins [3]. Frequently, these supernaturants are accompanied by urea, presumably for balancing stabilizing and destabilizing effects. The understanding of these effects on proteins caused by denaturants [4], supernaturants [5], and elevated pressure [6] has been the aim of many experimental and theoretical studies. On the theoretical side, molecular simulations are a powerful tool to get insight into molecular details of these processes [7–9]. Force field based simulations have shown to be especially versatile because of their advantage of being routinely applicable to systems of many thousand atoms on a time scale of up to microseconds. Thus, the study of denaturation of proteins [10], DNA [11], or RNA [12] by urea or the effects of urea on lipid bilayers [13] is possible, also the pressure denaturation of proteins [14]. However, their results are only as good as far as the force field gives a good description of physical reality. In general, force field quality has seen a continuous improvement over the last decades. This is largely due to the available computational capabilities. For example, free energy simulations have reached a point at which quantitative benchmarking to experimental work can be achieved [15]. Also, additional reference data has become accessible by quantum chemical methods. In the liquid state, ab initio molecular dynamics (AIMD) simulations [16] and embedded cluster reference interaction site method (EC-RISM) solvation theory [17,105] give molecular-scale insight into coordination structures, hydrogen bond numbers, and similar solvation properties, and also into electronic effects like the polarization response of solutes. Combining all these methods, we have recently developed a TMAO force field that gives a faithful description of TMAO in water [18]. Special attention has been given to the adaption of the force field to high pressure. High pressure conditions were challenging for force field development, because experimental data is often limited, if available at all. Therefore, quantum chemical electronic structure results at high pressure served as additional reference data for the force field adaption to high pressure.

Having an up-to-date force field for TMAO at hands, we are in need of a urea force field of similar quality for faithful simulations of mixtures of these two cosolutes. Standardized procedures for force field generation are available in the framework of general small molecule force fields like GAFF [19], but the resulting force fields do not describe liquid mixtures reliably. Most simulation studies involving aqueous urea solutions in the last decade relied on the Kirkwood-Buff force field (KBFF) of Weerasinghe and Smith [20]. This force field represented a milestone in urea force field development as it was able – contrary to previous force fields like OPLS [21] – to recover the nearly ideal mixing properties of urea and water, which is mandatory when it comes to studies of the effect of urea on protein thermodynamics [22].

Nevertheless, after nearly two decades it seems timely to readdress the force field description of urea. As we will show in this manuscript, the solvation shell structure of a urea molecule predicted by KBFF leaves room for improvement when compared to quantum chemical AIMD simulations. In this manuscript we present a new urea force field that aims at the improvement of KBFF along these lines. The development involved a synergistic combination of various experimental and computational methods: experimental densities at elevated pressures were obtained using vibrating tube densitometry and using X-ray absorption (XRA) measurements up to pressures of 5 kbar. Solvation properties at 1 bar and 10 kbar were determined by AIMD simulations and EC-RISM theory. Density extrapolations to 10 kbar, which are not trivial to achieve with the required precision, were performed independently by force field MD and by the perturbed-chain statistical associating fluid theory (PC-SAFT). For this purpose, PC-SAFT parameters of urea were required and determined in the present work. PC-SAFT parameters for water have been recently published with the focus to accurately describe high-pressure densities [23]. Based on these pure-component parameters, PC-SAFT allowed predicting the influence of urea concentration and of high pressure on aqueous mixture densities. Parameters have not been adjusted to aqueous mixture density data. Finally, advanced global optimization algorithms for the force field adjustment were employed. The resulting force field performs well in the whole studied pressure range. At ambient pressure, the mixing thermodynamics of urea/water is of similar quality as it is for the KBFF force field, while the new force field gives a better account of the solvation shell details from AIMD than KBFF. Experimental densities in the studied pressure and concentration range are accurately reproduced. At the very high pressure of 10 kbar, the solvation shell details still compare very well to AIMD.

## 2. Experimental methods and computational details

### 2.1. Vibrating tube densitometry

High pressure density data of aqueous mixtures of biomolecules is needed in many different fields of research like force field development [18,24,25], the analysis of X-ray scattering and reflectivity [23,26] or THz-spectroscopy [27]. Further, density data is often used to estimate parameters of equations of state or to validate their predictions [28,29]; densities are also required as input data if thermodynamic properties are modeled, e.g. viscosity [30], interfacial properties [31] or derivative properties [32]. Liquid densities can be experimentally determined at ambient pressure with standard equipment. Using a vibrating u-tube, only little sample volumes (approximately 2 mL) are needed to perform density measurements of very high accuracy [28,29]. However, density measurements become more complex at pressure in the kilobar regime and also the sample volume needed is large in many density measurement methods at increased pressure. Currently, literature data regarding the pressure influence on the density of aqueous urea solutions does not exist. Only experimental data of the density of aqueous urea solutions at atmospheric pressure and varying urea concentrations is available [33,34]. Consequently, new experimental data is needed addressing the pressure influence on the density of aqueous urea solutions. This data can then be used to validate model predictions, fit parameters, or prove the predictive accuracy of force fields.

For the preparation of the urea/water solutions, water from a Millipore water purification system was used. Urea was used from Merck with a purity of 99%. The components were weighed in using a Satorius laboratory balance with an accuracy of 0.0001 g in order to obtain solutions of the desired and defined composition. The density measurements were performed using an Anton Paar vibrating tube DMA 4200 M. The apparatus was calibrated using water and n-heptane and allows measurements with an accuracy of 0.1 kg/m$^3$ controlled temperature. Density measurements were performed at a temperature of 300.15 K ± 0.1 K for urea solutions with a molality of $m_{\mathrm{urea}} = 0.512$ and 1.045 mol urea per kg pure water, which is equivalent to a molarity of $c_{\mathrm{urea}} = 0.5$ and 1 mol/L urea solution, respectively. The measurement method was validated by measuring the density of aqueous sodium chloride solutions ($m_{\mathrm{NaCl}} = 1$ mol/kg, $T = 25^{\circ}C$, $p = 1$ to 400 bar) and ethanol/water mixtures ($\chi_{\mathrm{ethanol}} = 0.2$, $T = 25^{\circ}C$, $p = 1$ to 485 bar) and comparing to literature data [35,36]. The deviation between our own experimental density data and literature density values for these mixtures was smaller than 0.2%. Please note that these results are not shown here. Apparent molar volumes of urea were derived from the

density as

$$^{\phi}V_U = \frac{\rho_W - \rho}{c_U \cdot \rho_W} + \frac{M_U}{\rho_W} \quad (1)$$

with the solution density ρ, the pure water density $\rho_W$, the molar urea concentration $c_U$, and the molar mass of urea $M_U$.

### 2.2. Modeling with perturbed-chain statistical associating fluid theory (PC-SAFT)

In order to minimize experimental effort and consumption of chemicals, modeling density of aqueous biochemical systems at high pressure is highly desirable. On the one hand, mathematical fits and extrapolations can be used to describe and extrapolate the density of biochemical systems. However, parametrization of such simple models requires experimental data, and the accuracy of high-pressure extrapolation directly depends on the pressure range in which experimental data is available for parametrization. On the other hand, physics-based (non-empirical) thermodynamic models can be used to predict the density of biochemical systems at high pressure. The advantage of thermodynamic models is that often only pure-component data is needed for parametrization. Thermodynamic models consider physical relationships and therefore allow plausible predictions for various thermodynamic properties. It has been shown that – given a suitable thermodynamic model was applied – density predictions can be performed very accurately at different conditions concerning concentration, temperature and pressure up to the kilobar range, e.g., Ref. [37] shows an application to ionic liquids. In this work the equation of state PC-SAFT is used to predict high-pressure density data of aqueous urea solutions. PC-SAFT is well known to accurately predict densities of aqueous fluid systems. In previous works, PC-SAFT has already been used successfully to predict the concentration and temperature influence on the density of aqueous solutions of amino acids and peptides as well as osmolyte solutions [38,39]. Furthermore, PC-SAFT is well known to correctly model the pressure influence on the density of organic fluid systems, for example of 1-propanol + toluene mixtures at different concentrations and temperatures [40]. Besides modeling volumetric properties like density, it has been proved that PC-SAFT can also be used to predict energetic properties at high pressure. In 2012, PC-SAFT has been applied to predict the solubility of carbon dioxide in different imidazolium-based ionic liquids as a function of pressure [37]. In the present work, PC-SAFT is used to predict the pressure influence on the density of an aqueous urea solution. The results are completely predictive since no data of mixture density is needed. PC-SAFT parameters for water and urea were determined based on pure-component vapor pressures and liquid densities taken from literature. In order to predict the combined effects of urea concentration and pressure on aqueous urea solutions at ambient temperature, equation of state PC-SAFT in its original formulation by Gross and Sadowski [41,42] was used to predict the density of aqueous urea solutions of defined urea molality at a pressure range of 1 bar to 10 kbar. PC-SAFT calculates the residual Helmholtz free energy in a mixture by

$$A^{\text{res}} = A^{\text{HC}} + A^{\text{disp}} + A^{\text{assoc}}, \quad (2)$$

where $A^{\text{HC}}$, $A^{\text{disp}}$, and $A^{\text{assoc}}$ describe the Helmholtz-energy contributions due to hard-chain repulsion, dispersion, and association to the residual Helmholtz free energy $A^{\text{res}}$, respectively. Within PC-SAFT each molecule is described as a chain of spherical segments. The segments are defined by the segment diameter and the number of segments. The attractive interactions between the molecules are characterized by dispersion (van der Waals) and association (hydrogen bonding) forces. The number of association sites as well as the corresponding association-energy and the association-volume parameters are required for $A^{\text{assoc}}$. Standard Lorentz-Berthelot combination rules and Wolbach-Sandler mixing rules were used to describe mixtures based on the pure-component parameters. Modeling mixtures usually require the binary interaction parameter $k_{ij}$, which is standard procedure for PC-SAFT modeling [41,42]. PC-SAFT parameters for urea were fitted to sublimation-pressure data of pure urea [43–45]. A binary interaction parameter between water and urea was fitted to osmotic coefficients of urea in aqueous solution. The PC-SAFT parameters for water and for urea are summarized in Table S1 in the supporting information.

Finally, a binary interaction parameter $k_{ij}$ between water and urea was fitted to osmotic-coefficient data of aqueous urea solutions. The determined PC-SAFT pure-component parameters for water and for urea were used to predict liquid densities of binary water + urea solutions depending on pressure and urea concentration. The density of aqueous urea solutions at 1 bar and 298.15 K was predicted at molalities up to 4 mol/kg. Finally, it was the aim to use PC-SAFT to predict density of aqueous urea solutions up to very high pressures.

### 2.3. Density measurement from the absorption of X-rays

In the past, the absorption of X-rays has been successfully used to determine densities in a very high pressure regime of up to 1.3 Mbar (130 GPa) in diamond anvil cells, see e.g. [46,47] We recently adapted this technique to our high-pressure cell for X-ray reflectivity measurements [48] that can also be used in transmission geometry to perform absorption measurements. We showed that X-ray absorption measurements yield precise results for pressurized solutions in the kilobar regime [23]. The technique is based on the fact that the intensity $A_0$ of radiation with energy $E$ that passes matter with the linear absorption coefficient $\mu(E)$ over a distance $D$ is attenuated following Lambert-Beer's law as

$$A_1(D,E) = A_0 e^{-\mu(E)D} \quad . \quad (3)$$

The used X-ray energy is far away from any absorption edges of the involved elements. The linear absorption coefficient $\mu(E)$ depends on the density of the material as

$$\mu(p,E) = \rho(p)\sigma(E) \quad .$$

$\sigma(E)$ denotes the mass attenuation coefficient and $\rho(p)$ the homogeneous density. Since $\mu(E)$ depends thus on the pressure, the density is accessible in absorption measurements.

For experimental reasons, the set-up needs to be calibrated to a water reference [23]. After that, density changes can be determined relative to a known reference pressure. The reference density was determined in a vibrating-tube density meter at $p = 500$ bar. Finally, the linear absorption coefficient $\overline{\mu}_s(p)$ of the sample can be determined from

$$\overline{\mu}_s(p) = \frac{M(p) + c}{M(p_0) + c}\left[\frac{\overline{\mu}_s(p_0)d_s + \overline{\mu}_w(p_0)d_w}{d_s}\right] - \frac{\overline{\mu}_w(p)d_w}{d_s} \quad . \quad (4)$$

Here, $M(p) = \sum \ln \frac{I_0}{I_1}$ is the integrated value of the measured signals in ionization chambers before and after the sample in the measured energy range at a given pressure and $d_s$ and $d_w$ indicate the absorbing length of the sample and a small additional layer of pressure-transmitting liquid, respectively. The constant $c$ is specific for the instrument and can be determined from the water calibration, $\overline{\mu}_s(p_0)$ and $\overline{\mu}_w(p)$ are calculated from the reference density, the pressure-dependent density of water [49] and the mass attenuation coefficients $\sigma$ [50]. A simple division by the mass attenuation coefficient gives then the sample density as

$$\rho_s(p) = \frac{\overline{\mu}_s(p)}{\sigma_s} \quad .$$

More details of the experimental setup and the analysis are given in Ref. [23]

Experiments were performed at beamline BL8 of DELTA at beam energy between 16.81 keV to 16.91 keV [51]. Urea solutions with $c = 1$ mol/L were prepared by weighing the appropriate amount of urea (VWR) and

adding water (MilliQ, resistivity $R = 18.2$ MΩ cm) to the desired volume. The temperature was set to 298.15 K, the pressure stability was below 1%.

### 2.4. Ab initio molecular dynamics simulations

The AIMD [16] simulations were carried out using the `CP2K 5.0` ab initio molecular dynamics package [52] employing the Born-Oppenheimer potential energy surface as generated by the `Quickstep` module [53]. The RPBE density functional [54], as implemented in the libxc [55] library, was used to describe the electronic structure enhanced by the D3 dispersion correction [56] using two-body interactions and zero-damping. The resulting RPBE–D3 approach has been demonstrated repeatedly to be successful in accurately describing water clusters, bulk water and aqueous solutions including high pressure and supercritical conditions [18,57–68].

Within the Gaussian and plane waves (GPW) scheme [69] underlying `Quickstep`, a triple-ζ basis set with polarization functions [70], namely TZV2P, together with a plane wave cutoff of 500 Ry to represent the electronic charge density was used; the NN50 scheme was utilized to smoothen the electron density as well as the derivatives. Norm-conserving separable dual-space Gaussian pseudopotentials [71,72] were used to implicitly describe the effects of the core electrons. One urea molecule together with 110 water molecules as hosted in a periodic cubic supercell was simulated at two densities corresponding to 1 bar and 10 kbar. The experimental density of 0.5 mol/L urea at 1 bar (1004.88 g/L, this work) is reproduced by the system with a box length of 14.9984 Å, which yields a concentration of 0.492 mol/L. The density at 10 kbar was obtained by fitting the densities of the new force field, which was optimized for 1 bar, to the equation of state (Eq. (7)) and using the value of the fit at 10 kbar. The resulting density of 1247.03 g/L leads to a box length of 13.9569 Å and a concentration of 0.611 mol/L. The canonical ensemble at 300 K was established using massive Nose-Hoover chain thermostats [73] using a chain length of 5 and a time constant of 16.67 fs. The Born-Oppenheimer AIMD equations of motion were integrated with a time step of 0.5 fs. For the subsequent microcanonical simulations, 20 initial configurations were sampled every 3 ps from the NVT simulations at 1 bar as well as at 10 kbar. These NVE simulations were propagated for 20 ps each and used to generate the data shown.

### 2.5. Integral equation theory

EC-RISM calculations for urea followed closely the procedures developed earlier for TMAO [18], i.e. without explicitly placed water molecules and chosing a level of theory that has been appropriately benchmarked. Briefly, dipole moment and atomic charges of urea were calculated using the B3LYP/6–311 + G(d,p) level of theory as implemented in Gaussian 03 Rev. E.01 [74] applying the CHelpG fitting method for the charges. The geometry was optimized using the same level of theory employing the polarizable continuum model (PCM) with default settings for modeling a water environment. For the EC-RISM single point calculations as a function of pressure water was represented based on the SPC/E model by solvent susceptibilities taken from 1D RISM/HNC (hypernetted chain) or from MD. The closure used in 3D RISM calculations was the third-order partial series expansion (PSE-3). The 3D grid resolution of 0.3 Å and a solvent buffer of 25 Å resulted in a a grid of 90 × 88 × 84 grid points. The EC-RISM convergence criterion was set to 0.01 kcal/mol, and the 3D RISM threshold for the maximum norm change of the direct correlation function between two successive steps was set to 0.000001. The final energy calculation was performed using 30 Å of solvent buffer resulting in a grid size of 106 × 104 × 100. For the Lennard-Jones potential the force field parameters summarized below were used.

### 2.6. Force field molecular dynamics simulations

The simulations were performed using the GROMACS 2016.3 package [75]. Analyses were performed with GROMACS and in-house code, except for the spatial distribution function (SDF) determination, where we used `TRAVIS` [76] and `VMD` [77]. The Lennard-Jones parameters were mixed using the Lorentz-Berthelot combination rule. The Lennard-Jones and real-space Coulomb interactions were cut off at 1.0 nm, and the periodic electrostatics were calculated via smooth particle-mesh Ewald summation [78] with a lattice spacing of 0.12 nm. Nonbonded 1–2 and 1–3 interactions in urea were excluded. A time step of 2 fs was used, while all bond lengths were kept constant via the SETTLE [79] (water) and LINCS [80] (urea) algorithms. For temperature control the stochastic velocity rescaling thermostat [81] was set to 298.15 K or 300 K with a time constant of 1 ps. The pressure was set via the Berendsen barostat [82] with a time constant of 1 ps for equilibration and via the Parrinello-Rahman barostat [83] with a time constant of 2 ps for production runs. The TIP4P/2005 water model [84] was used in all simulations except for short reference simulations of the KBFF urea model [20] in SPC/E water [85]. In order to calculate the densities, apparent molar volumes (AMV), and activity coefficient derivatives at 1 bar, 32 urea concentrations between 1 and 9 mol/L were simulated for 150 ns each. For the density simulations of urea solutions as a function of pressure, 19 urea and 2055 water (0.5 mol/L), and 39 urea in 2037 water (1 mol/L) were simulated for 10 ns. A newly optimized force field was developed based on the fitting of the experimental density of urea in the concentration range up to 9 mol/L and of solvation shell characteristics derived from AIMD. Details of the optimization procedure, which employed a differential evolution algorithm [86], are given in the supporting information. The optimized force field parameters are shown in Tables 1 and 2, where the bonded parameters are a hybrid between the KBFF [20] and GAFF [19] parameters (see the supporting information for details).

From the resulting force field, the concentration- and pressure dependent densities and apparent molar volumes were determined. Furthermore, the activity coefficient derivatives in the molarity scale $y_{UU}$ were calculated as

$$y_{\mathrm{UU}} = \left(\frac{\partial \ln y_{\mathrm{U}}}{\partial \ln c_{\mathrm{U}}}\right)_{p,T} = \frac{c_{\mathrm{U}}\,(G_{\mathrm{UW}} - G_{\mathrm{UU}})}{1 + c_{\mathrm{U}}\,(G_{\mathrm{UU}} - G_{\mathrm{UW}})} \tag{5}$$

where $c_{\mathrm{U}}$ is the molar urea concentration, and $G_{ij}$ are the Kirkwood-Buff

**Table 1**
Bonded parameters of the new urea force field developed in this work. All bond lengths are constrained. The bond angle potential is harmonic: $V_{\mathbf{a}}(\phi) = \frac{1}{2}k_{\phi}(\phi - \phi_0)^2$. The dihedral potential is of the form: $V_d(\theta) = k_{\theta} \cdot (1 + \cos(n\theta - \theta_S))$.

| Bonds | r/nm |
|---|---|
| C–O | 0.1229 |
| C–N | 0.1335 |
| N–H | 0.1010 |

| Bond angles | $\phi_0$/deg. | $k_{\phi}$/(kJ mol$^{-1}$ rad$^{-2}$) |
|---|---|---|
| C–N–H | 120.0 | 390 |
| H–N–H | 120.0 | 445 |
| O–C–N | 121.4 | 730 |
| N–C–N | 117.2 | 670 |

| Dihedral angles | $\theta_S$/deg. | $k_{\theta}$/(kJ mol$^{-1}$) | n |
|---|---|---|---|
| O–C–N–H | 0.0 | 8.368 | 1 |
| O–C–N–H | 180.0 | 10.460 | 2 |
| N–C–N–H | 180.0 | 10.460 | 2 |
| N–N–C–O | 180.0 | 43.932 | 2 |
| C–H–N–H | 180.0 | 4.184 | 2 |

**Table 2**
Lennard-Jones parameters and partial charges of the new urea force field developed in this work. $\mathbf{H^{cis}}$ and $\mathbf{H^{trans}}$ are the hydrogen atoms on the same and opposide side of a C–N bond as the oxygen atom respectively.

| | $\sigma$/nm | $\varepsilon$/(kJ mol$^{-1}$) | q(1 bar)/e | q(HPFF-10 kbar)/e |
|---|---|---|---|---|
| C | 0.36039 | 0.35982 | 0.6068 | 0.6389 |
| $H^{cis}$ | 0.11333 | 0.06569 | 0.4026 | 0.4150 |
| $H^{trans}$ | 0.11333 | 0.06569 | 0.4421 | 0.4565 |
| N | 0.34452 | 0.51114 | −0.8400 | −0.8603 |
| O | 0.31377 | 0.59432 | −0.6162 | −0.6613 |

integrals (KBIs) [87]. There are many different ways to approximately determine the KBIs for the limit of an infinitely large, open system. Ganguly and van der Vegt have previously developed an empirical correction to radial distribution functions (RDFs), which fixes the asymptotic deviation of finite- and closed-system RDFs from unity at large distances by accounting for the local excess of species $i$ around $j$ [88]. With other methods, the KBIs can be calculated directly from the particle number fluctuations in subvolumes of the simulation box, even though the particle number in the total system is constant. In this work, we calculate KBIs using the method by Cortes-Huerto et al. [89], which is based on work by Krüger et al. [90] We note that it was recently shown that, out of the currently available corrections, the method by Ganguly and van der Vegt yields the most accurate results [91]. In the method by Cortes-Huerto et al., the KBIs of cubic subboxes with volume $V$ of the simulation box with total volume $V_0$ were calculated as

$$G_{ij}(V, V_0) = V\left(\frac{\langle N_i N_j\rangle - \langle N_i\rangle\langle N_j\rangle}{\langle N_i\rangle\langle N_j\rangle} - \frac{\delta_{ij}}{\langle N_i\rangle}\right) \tag{6}$$

with the molecule numbers $N_i$ and angular brackets denoting time averages. Next, the $G_{ij}(V, V_0)$ are multiplied with the ratios of the lengths of the cubic subboxes and the simulation box $\lambda = \sqrt[3]{V/V_0}$. The extrapolated KBIs of the open system are then the slope of $\lambda G_{ij}(\lambda)$ fitted in the linear region between $\lambda = 0.1$ and $\lambda = 0.2$.

### 2.7. Equation of state

A simple to use equation of state was derived from the densities of the 0.5 mol/L urea solutions as a function of pressure derived with the optimized force field. The functional form was chosen according to a high-pressure equation of state for pure water in Ref. [92] as

$$\rho^{\mathrm{EoS}}(p) = \rho(1\ \mathrm{bar}) + a_0 \ln\frac{a_1 + p}{a_1 + 1\ \mathrm{bar}}. \tag{7}$$

### 2.8. High-pressure force field

The high-pressure adjustment of the optimized urea force field was done by scaling all partial charges of the urea force field as described in Ref. [18]. The pressure-dependent HP versions were obtained by scaling the partial charges such that the relative dipole moment increment between the normal pressure FF and the high-pressure FF is identical to the pressure induced changes in the EC-RISM dipole moments.

## 3. Results and discussion

### 3.1. PC-SAFT modeling at 1 bar

The PC-SAFT pure-component parameters of water allow modeling the experimental data of pure water with an average relative deviation (ARD) of 0.011% for the vapor pressure, 0.1066% for the saturated liquid density and 0.1293% for the liquid density up to 10 kbar, respectively. The PC-SAFT modeling results for the sublimation pressure of urea are shown in Fig. 1. The ARD for the sublimation pressure is

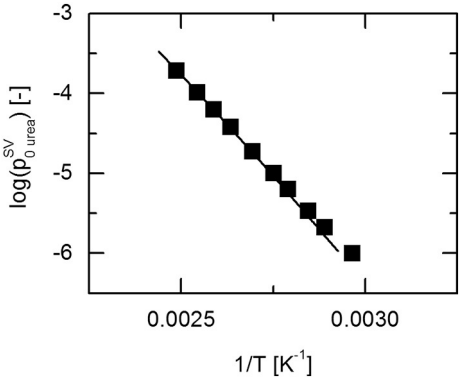


**Fig. 1.** Logarithm of the sublimation pressure of urea plotted against the inverse temperature in 1/K. Squares: Literature data [43–45], line: PC-SAFT modeling results using the parameters from Table S1 in the supporting information.

10.08%, which is a reasonable result compared to other studies which use sublimation-pressure data to fit PC-SAFT parameters [93–95]. The parameter set for urea obtained from fitting to sublimation-pressure data was used to calculate the density of hypothetically-liquid supercooled urea at 298.15 K. This density was found to be in the range of 20.1 mol/L, which is in agreement to experimental density of solid urea at 298.15 K [96].

PC-SAFT modeling predicted the osmotic coefficient of urea/water with an ARD of 0.36%. The density of aqueous urea solutions at 1 bar and 298.15 K at molalities up to 4 mol/kg was predicted with an ARD of 0.48% (data shown below together with the force field results). We note that these results are predictive in the sense that no mixture densities of water/urea solutions were used to fit any of the PC-SAFT parameters. Thus, PC-SAFT predicts the combined effect of pressure and concentration on liquid density.

The comparison of the measured density of a 1 mol/L urea solution to established experimental data from literature [33] shows that the experiments and the MD simulations give very good results at 1 bar pressure. The change of the AMV with urea concentration is very weak. The PC-SAFT results are also resonable, but give an AMV that is significantly varying with urea concentration.

### 3.2. Solvation at 1 bar

Fig. 2 shows details of the solvation shell structure of urea obtained by AIMD, by EC-RISM, and by the newly derived force field, which will be discussed below in the next paragraph. Fig. 2a shows the radial distribution functions (RDFs) between every urea atom and the water oxygens. The oxygen and carbon atom show a pronounced first and second solvation peak. In the nitrogen RDF the first peak is only weakly pronounced and is followed by two small peaks. In the RDFs of the hydrogens, the first peak is very weak with a peak height below 1 and is followed by two weak maxima.

The AIMD and EC-RISM spatial distribution functions, Fig. 2b, demonstrate that the water oxygen in the first solvation shell populates regions that are compatible with this water molecule forming hydrogen bonds either as a donor to N or O or as an acceptor of the hydrogens. Fig. 2c shows the hydrogen bonding coordination at 1 bar. The probability distributions for the hydrogen bond number of the individual hydrogen bonding sites show that urea acceptor bonds – out of which the vast majority involves the urea oxygen – slightly dominate over urea donor hydrogen bonds, which are formed by cis and trans hydrogens with nearly the same probability.

### 3.3. Force field optimization

The new force field reproduces all studied solvation shell properties

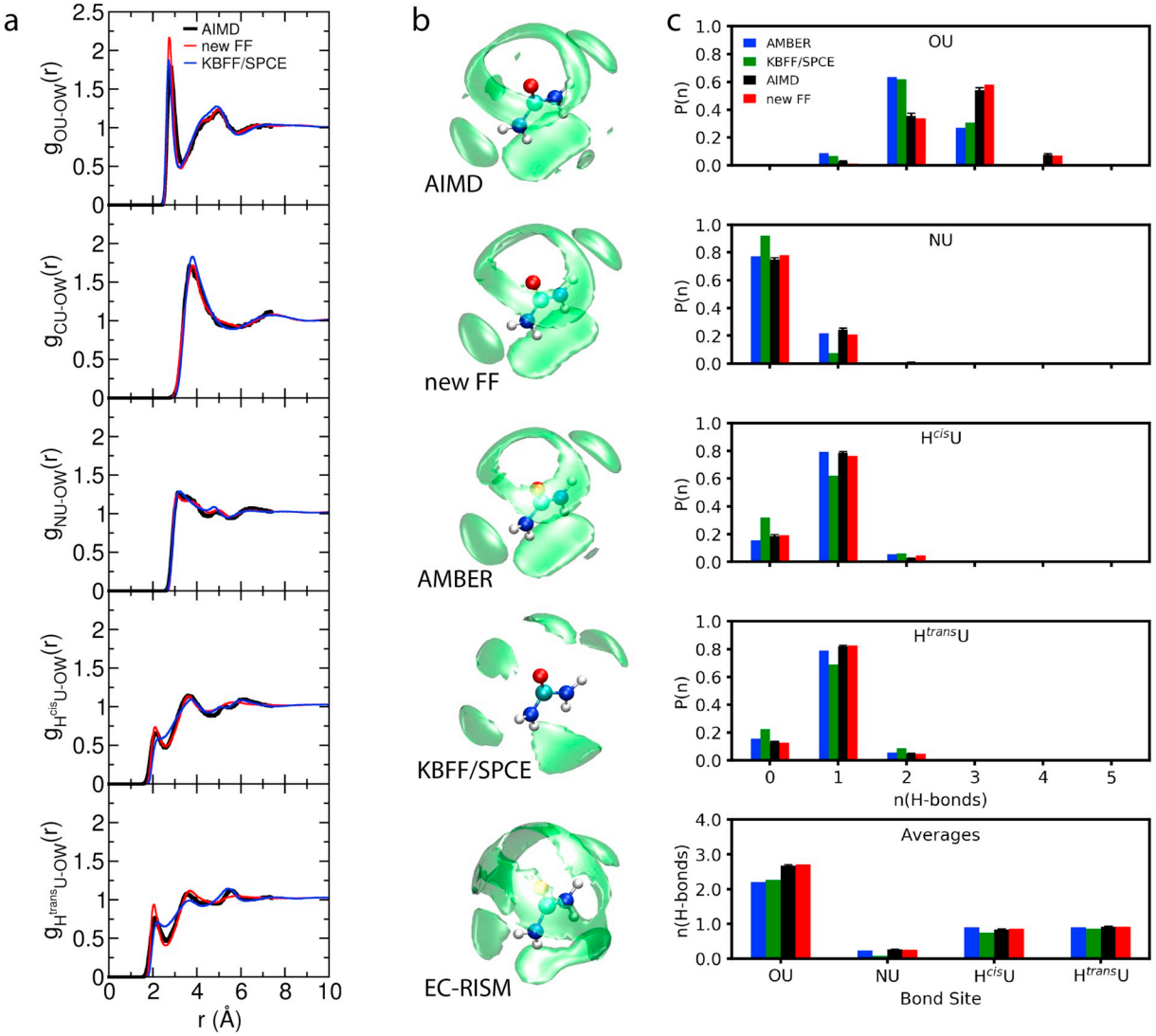


**Fig. 2.** a: Radial distribution functions for AIMD and the new FF at 1 bar between urea atoms. b: Spatial distribution functions (SDFs) of the water oxygen density around urea at 1 bar. The isosurface corresponds to twice the bulk water density in MD simulation results and to 2.6 times the bulk water density in the EC-RISM results for easier comparison of topographic features. The MD distributions were symmetrized with respect to the vertical and horizontal symmetry plane and subsequently smoothed. c: Probability distributions of the number of urea-water hydrogen bonds per urea donor/acceptor site at 1 bar.

of a single urea molecule in water with very high quality, see Fig. 2: RDFs, SDFs, and hydrogen bond coordination. The good agreement with AIMD solvation properties demonstrates that the new force field is capable of describing the solvation of one urea molecule very well. However, the development of the KBFF urea force field showed that is is non-trivial to also reproduce the thermodynamic mixing properties of concentrated urea solutions, which came out to be very non-ideal with force fields like OPLS or AMBER [22]. In our force field optimization, we took care to also get a good account of urea solutions up to concentrations of 9 mol/L, where intermolecular urea-urea interactions play a crucial role for the mixing thermodynamics. Concentration dependent properties are shown in Fig. 3. The densities and the AMV of urea up to $c_{\mathrm{urea}} = 9$ mol/L agree very well with the experimental data, which renders our force field suitable for high-pressure studies. The activity coefficient derivative obtained with the new force field from Kirkwood-Buff theory compares well to the result we obtained with the KBFF force field. The shape of the nearly parabolic experimental curve is reproduced by our force field, however, the agreement is not perfect: the minimum is slightly too low ($-0.08$ instead of $-0.05$) and is shifted to higher urea concentration (4 mol/L instead of 2.5 mol/L). Compared to OPLS or AMBER [22], this disagreement is minor and the deviations from ideality are still rather small. The dielectric constant is significantly underestimated: the force field predicts a value around 60 with almost no sensitivity to the urea concentration, whereas the experimental result increases from 78 for pure water to 95 at 9 mol/L urea concentration [97]. This agreement is not good, but KBFF also results in no significant change of the dielectric constant with urea concentration. The better agreement of KBFF with the experimental data is merely an effect of the underlying water model: SPC/E water, the model for which KBFF was developed has a higher dielectric constant of 70 at standard conditions compared to TIP4P/2005, which has a dielectric constant of 58. The adiabatic compressibility $\kappa_S$ is in nearly quantitative agreement with the experimental data [98]. The diffusion constant derived from the mean squared displacement of urea decreases with urea concentration similar to KBFF. The experimental data, which also shows this decrease, is in in better quantitative agreement with the KBFF data. However, the diffusion constants in the simulations are influenced by the shear viscosity of the underlying water model. In fact, TIP4P/2005 predicts a viscosity of $\eta = (0.855$ mPa s) that is in good agreement with the experimental value of 0.896 mPa s [99], which is underestimated by SPC/E (0.725 mPa s). Since a lower viscosity will allow for faster diffusion of solutes, this better performance of KBFF might be a

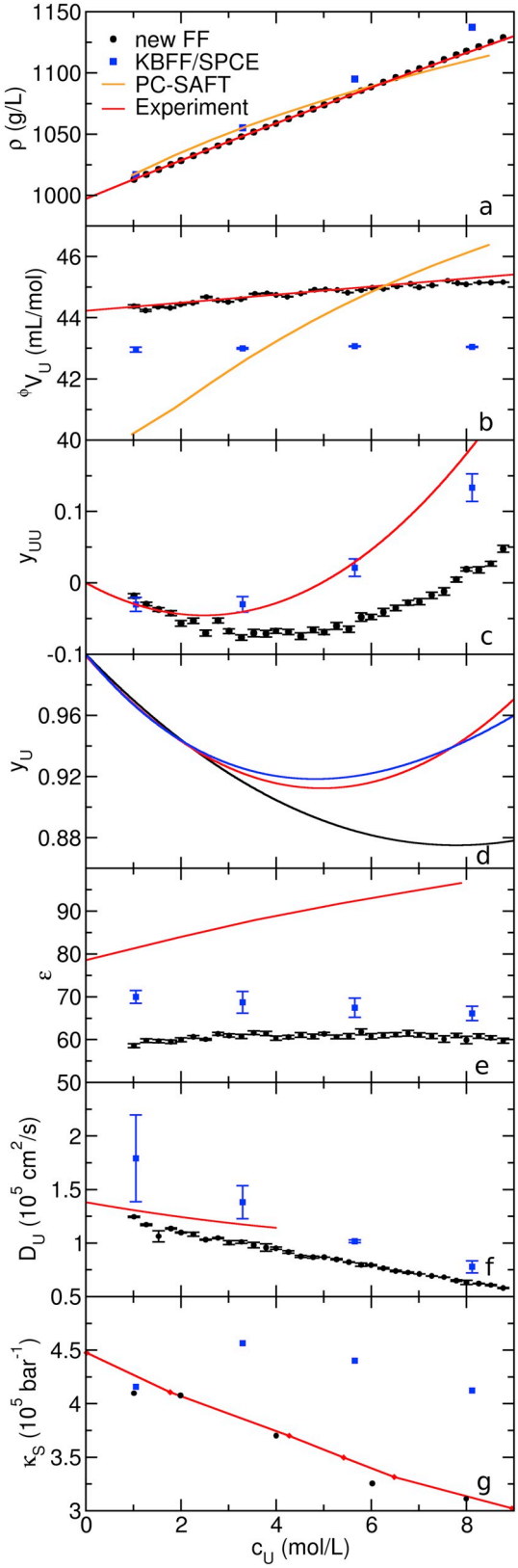


**Fig. 3.** Properties of aqueous urea solutions of the new force field and experimental reference data at 1 bar and 298.15 K as a function of the molar concentration $c_U$. a: Solution density. b: Apparent molar volume of urea. c: activity coefficient derivatives of urea in the molarity scale. d: Activity coefficient of urea by analytic integration of the fitted $y_{UU}$ from simulations. e: Static dielectric permittivity calculated using the method in Ref. [100]. f: Diffusion coefficient of urea calculated from the root mean squared displacement. g: Adiabatic compressibility of the system, converted from isothermal compressibilities, which were calculated from the finite differences of the density at 1, 100, and 200 bar. Experimental data was taken from Refs. [33] (a, b), [101] (c, d), [97] (e), [102] (f), and [98] (g).

consequence of the low viscosity of SPC/E water.

We conclude that our force field is able to capture single particle solvation properties as well as collective solution properties at finite concentrations very well. The excellent performance of KBFF in the prediction of thermodynamic mixing properties is matched, but since our force field was designed to also reproduce the properties of the water solvation shell, it gives a more realistic account of the solution structures than KBFF. Thus, we have a reliable force field for 1 bar, and the excellent prediction of densities make it highly suitable for the following high-pressure studies.

### 3.4. High-pressure densities of urea solutions

Vibrating tube densitometry up to 500 bar yields a density increase from 1005 g/L at 1 bar to 1025 g/L at 500 bar for the $c_{urea}$ = 1 mol/L solution, see Fig. 4a. The experimentally determined apparent molar volumes of urea are in the range of 43–44 mL/mol and show no significant pressure dependence. PC-SAFT slightly overpredicts the density and underestimates the AMV accordingly. The MD simulations show very good agreement with a maximum deviation of 0.7 g/L at 500 bar. The apparent molar volumes are also in good agreement within the estimated errors. The difference between PC-SAFT and the force field is 13 g/L or about 1% at 10 kbar. Given that PC-SAFT parameters were not fitted at all to mixture density data, the PC-SAFT predictions can be considered as very satisfying results.

Results from XRA, which gives experimental access to densities at much higher pressure up to 5 kbar, are shown in Fig. 4b. The error of the AMV in the XRA experiments is in the range of 10 mL/mol, which is a good precision given that the AMV is related to the absolute density difference between urea solution and water. At pressures below 200 bar, the error bars are large, because at these low pressures a small amount of air can still produce artifacts. At 5 kbar, a more drastic density increase up to 1159 g/L is observed. PC-SAFT and MD simulations both give a very accurate account of the density in this range. Also the AMV, which is still rather insensitive to the increased pressure, is well reproduced. This agreement is excellent, considering that no high-pressure experimental calibration went into the force field and even no mixture density data at all were used to fit the PC-SAFT parameters. Therefore, an extrapolation to 10 kbar can be done with high confidence. The density at 10 kbar is predicted to be 1253 g/L by MD and 1244 g/L by PC-SAFT. The good agreement gives again further credibility to our extrapolation. The AMV predicted by MD slightly drops to 42 mL/mol, while the PC-SAFT AMV increases to 45 mL/mol. Considering the approximative nature of PC-SAFT and the force field, this is still good agreement.

For the AIMD simulations with 110 water molecules and one urea molecule we require the density of a $c_{urea}$ = 0.5 mol/L urea solution at 10 kbar. While there is no XRA data available at this concentration, the assessment of the validity of our 10 kbar extrapolation also justifies the extrapolation at $c_{urea}$ = 0.5 mol/L. Detailed results are shown in the supporting information, where we note that the extrapolated density at 10 kbar is 1247.03 g/L.

### 3.5. Solvation at 10 kbar

Fig. 5a shows the radial distribution functions between every urea atom and the water oxygens. All RDFs show an increase in coordination: the first peaks are higher than the respective peaks in the

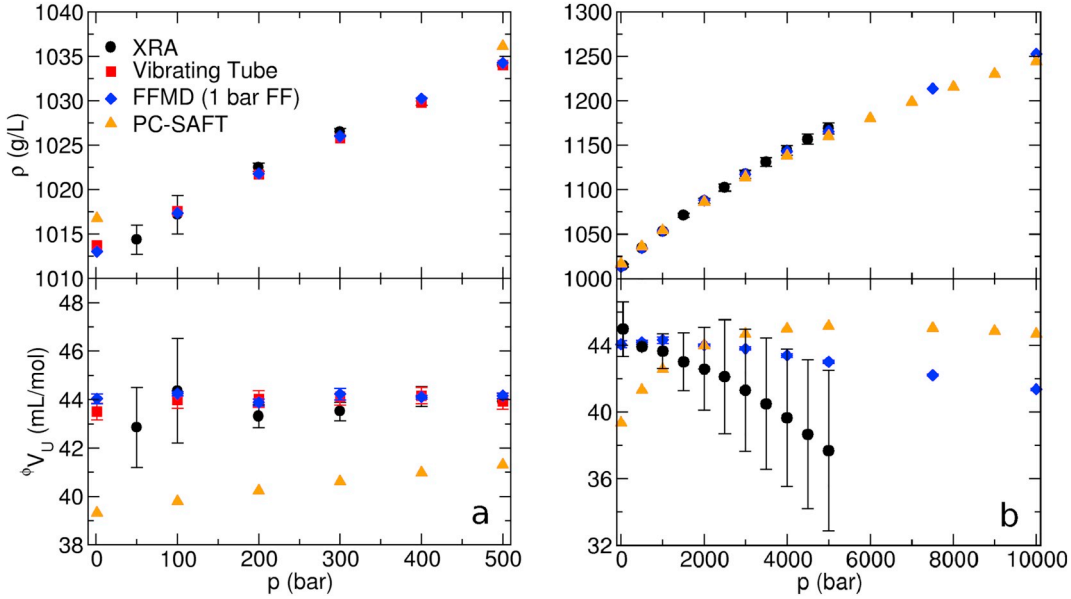


**Fig. 4.** Solution densities ρ and apparent molar volumes of urea $^{\phi}V_U$ of a 1 mol/L aqueous urea solution at 298.15 K for pressures up to 500 bar (a) and 10 kbar (b). Circles: XRA, squares: vibrating tube, diamonds: force field MD, triangles: PC-SAFT.

corresponding 1 bar RDF. This is most prominent for the urea nitrogen. The RDF features beyond the first peak all become more pronounced. The force field results are in excellent agreement with the AIMD data with regard to the positions and heights of the peaks. The most significant deviations are observed in the urea oxygen RDF in the region of the first minimum. The spatial distribution functions, shown in Fig. 5b, show that compared to 1 bar more regions of the first solvation shell in the vicinity of the urea molecule become populated. AIMD and force field simulation results are in excellent agreement. The solvation shell prediction by EC-RISM is more isotropic than predicted by the simulations, similar to the results at 1 bar.

Fig. 5c shows the hydrogen bonding coordination at 10 kbar. The probability distributions for the hydrogen bond number of the individual hydrogen bonding sites show that urea acceptor bonds – where the vast majority involves the urea oxygen – slightly dominate over urea donor hydrogen bonds, which are formed by cis and trans hydrogens with nearly the same probability. The agreement between AIMD and force field MD is excellent for studied properties at 10 kbar even though no scaled charges, unlike the TMAO case, were used.

The molecular dipole moment of urea as a function of pressure as calculated with EC-RISM is shown in Fig. 6. For the hypernetted chain (HNC) closure, the dipole moment changes only marginally from 7.06 D at 1 bar to 7.16 D at 10 kbar, which is consistent with earlier work, where it was shown that HNC is insufficient to reproduce the pressure-induced polarization of the solute [18]. For the solvent susceptibilities from MD simulations, the dipole moment changes rapidly with pressure from 6.68 D at 1 bar to 7.00 D at 3 kbar, followed by a very small decrease at 4 kbar and a jump to 7.08 D at 5 kbar. Furter increasing the pressure has little effect, increasing the dipole moment to 7.10 D at 10 kbar. The same qualitative behavior has been observed for the solute TMAO [18]. This implies also the apparent discontinuity at around 4 kbar, for which we have no explanation.

The dipole moments deduced from AIMD also show an increase of the dipole moment to 7.55 D at 10 kbar relative to the dipole moment of 7.33 D at 1 bar. Thus, it seems logical to scale the urea force field's partial charges with increasing pressure for an even better account of the behavior at high pressures.

### 3.6. High pressure force field

In the case of urea it is evident that our force field, which was designed to properly describe urea solutions at 1 bar, is able to reproduce the solvation details at 10 kbar. This is in remarkable contrast to TMAO, where we observed that a 1 bar nonpolarizable force field does not fully account for the 10 kbar solvation [18]. This was traced back to the lacking increase of electronic polarization in water under high pressure. Accounting for this increase by explicitly pressure-dependent charges such that the dipole increases similar to the dipole obtained from EC-RISM, we derived a force field that we labeled labeled as HP-FF. This HP-FF gave a better account for the increased hydrogen bonding of TMAO at high pressure. For urea, the unmodified ambient pressure force field already works well, even if the dipole moment increase at high pressure is not accounted for. In this light, it is interesting to see if the HP-FF for urea performs even better. Concerning the density, the HP-FF gives nearly the same results as the 1 bar FF (data not shown). At 10 kbar and 1 mol/L urea, the two force fields differ by only 0.7 g/L. However, the urea HP-FF reproduces the AIMD results worse than the unadjusted 1 bar force field, see Fig. 5. Weerasinghe and Smith have observed that the dipole moment of urea is only a weak indicator for the mixing thermodynamics [20]. Apparently, it is also not necessary to account for the correct dipole increase for a good account of the solvation properties of a single urea molecule.

The physical reason for this apparent discrepancy between TMAO and urea remains speculative, though. One aspect could be the strong basicity of TMAO which could lead to some degree of electron transfer between water and the solute. A fixed-charge force field, unable to reproduce such an effect, would in this case compensate for the deficiency by a tendency to overpolarization, which therefore appears unnecessary in the case of urea. For all practical purposes we suggest working with unscaled urea charges.

In principle, polarization could also be included by using the Drude particle formalism or atomic dipole polarizabilities. Inclusion of such terms in high-level force fields certainly has the potential for an overall improvement of the simulation quality (see for example the success of modern high-level water model like MBPOL [103]). This comes however at the cost of the development of a total new force field that will be furthermore computationally less efficient. Our observation supports

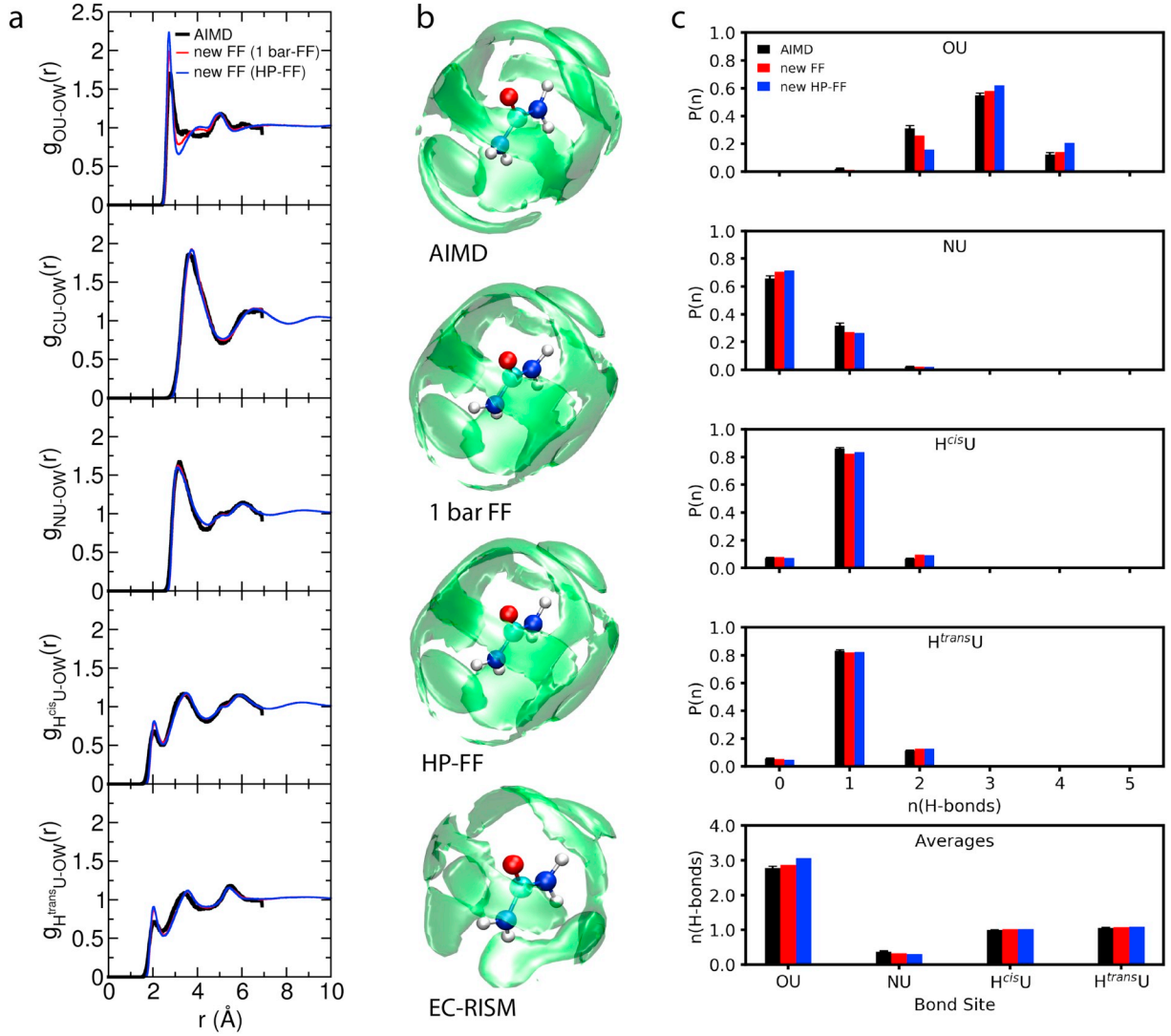


**Fig. 5.** Solvation structure at 10 kbar. a: Radial distribution functions for AIMD, the new FF, and its high-pressure modification (HP-FF) at 10 kbar between urea atoms and water oxygen. b: SDFs of the water oxygen density around urea at 10 kbar. The isosurface corresponds to twice the bulk water density in MD simulation results and to 2.6 times the bulk water density in the EC-RISM results for easier comparison of topographic features. The MD distributions were symmetrized with respect to the vertical and horizontal symmetry plane and subsequently smoothed. c: Probability distributions of the number of urea-water hydrogen bonds per urea donor/acceptor site at 10 kbar.

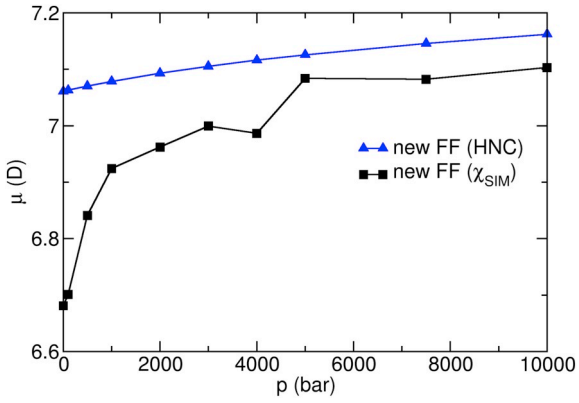


**Fig. 6.** EC-RISM dipole moments of urea as a function of pressure using the Lennard-Jones parameters of our new force field for the hypernetted chain (HNC) closure and susceptibilities from MD simulations of SPC/E water ($\chi_{SIM}$).

the use of a non-polarizable urea force field at a level of accuracy that is sufficient for the study of cosolute and high pressure effects.

## 4. Conclusions and outlook

In this work we present a new force field for urea based on comparison to experimental, ab initio molecular dynamics, and quantum chemical data at ambient and high hydrostatic pressures. Developing the force field required new experimental data up to high pressure. For this purpose, vibrating-tube measurements up to 500 bar and X-ray absorption measurements up to 5 kbar were performed for urea-water mixtures. These data were validated by PC-SAFT, which was used in a predictive mode as no mixture density data was used to fit the parameters. Based on such cross-validated data, the force field for urea was developed in this work. The newly derived force field shows improved performance compared to previously used force fields. It gives an accurate account for solvation on a single molecule level and for mixing effects, which leads to well behaved thermodynamic properties. The densities of urea-water mixtures that were obtained with the new force field were in accurate agreement to experimental data and PC-SAFT in

broad ranges of pressure and urea concentrations. Thus, our force field is ideally suited for future simulation studies of biomolecules in the presence of urea. The force field is optimized along similar lines as our previously reported TMAO force field, which paves the road for reliable studies of urea/TMAO mixtures, where TMAO was observed to prevent urea adsorption at the protein [104], even at elevated pressures.

To our surprise, explicit account for pressure-dependent polarization is not necessary, which is in contrast to our observations for TMAO. It is closer in behavior to water, for which no pressure dependent polarization needs to be accounted for. A link of the molecular structure of a solute molecule to the need (or lack of need) for pressure-dependent force fields is currently not known to us. This will be of high relevance when it comes to protein force fields, which are optimized to describe subtle balances of different forces such that macromolecular conformational equilibria are correct. It may turn out that there is no pressure adaption of the partial charges required and that force fields for standard pressures are appropriate for high-pressure simulations studies.

## Acknowledgement

This research was funded by Deutsche Forschungsgemeinschaft within the research unit FOR 1979. GS, SK, and DM also acknowledge support from the Cluster of Excellence RESOLV (EXC 2033, project number 390677874) funded within Germany's Excellence Strategy. We acknowledge Ralph Wagner for help with the experiments at beamline BL8 and the DELTA crew for providing synchrotron radiation. Members of the research unit are acknowledged for many insightful discussions. We thank Christian Sternemann, Mirko Elbers, Jennifer Bolle, Göran Surmeier, and Shaohan Zhu (all Technische Universität Dortmund) for supporting the absorption experiments.

## Appendix A. Supplementary data

Supplementary data to this article can be found online at https://doi.org/10.1016/j.bpc.2019.106260.

## References

[1] P. Yancey, M. Clark, S. Hand, R. Bowlus, G. Somero, Living with water stress: evolution of osmolyte systems, Science 217 (1982) 1214–1222.
[2] K. Julius, J. Weine, M. Berghaus, N. König, M. Gao, J. Latarius, M. Paulus, M.A. Schroer, M. Tolan, R. Winter, Water-mediated protein-protein interactions at high pressures are controlled by a deep-sea osmolyte, Phys. Rev. Lett. 121 (2018) 38101.
[3] P.H. Yancey, Organic osmolytes as compatible, metabolic and counteracting cytoprotectants in high osmolarity and other stresses, J. Exp. Biol. 208 (2005) 2819–2830.
[4] C. Tanford, Isothermal unfolding of globular proteins in aqueous urea solutions, J. Am. Chem. Soc. 86 (1964) 2050–2059.
[5] I. Baskakov, D.W. Bolen, Forcing thermodynamically unfolded proteins to fold, J. Biol. Chem. 273 (1998) 4831–4834.
[6] K. Akasaka, Probing conformational fluctuation of proteins by pressure perturbation, Chem. Rev. 106 (2006) 1814–1835.
[7] L. Hua, R. Zangi, B.J. Berne, Hydrophobic interactions and dewetting between plates with hydrophobic and hydrophilic domains, J. Phys. Chem. C 113 (2009) 5244–5253.
[8] B. Moeser, D. Horinek, Unified description of urea denaturation: backbone and side chains contribute equally in the transfer model, J. Phys. Chem. B 118 (2013) 107–114.
[9] E. Schneck, D. Horinek, R. Netz, Insight into the molecular mechanisms of protein stabilizing osmolytes from global force-field variations, J. Phys. Chem. B 117 (2013) 8310–8321.
[10] L. Hua, R. Zhou, D. Thirumalai, B.J. Berne, Urea denaturation by stronger dispersion interactions with proteins than water implies a 2-stage unfolding, Proc. Natl. Acad. Sci. U. S. A. 105 (2008) 16928–16933.
[11] E.A. Oprzeska-Zingrebe, J. Smiatek, Preferential binding of urea to single-stranded DNA structures: a molecular dynamics study, Biophys. J. 114 (2018) 1551–1562.
[12] J.C. Miner, A.E. Garcia, Equilibrium denaturation and preferential interactions of an RNA tetraloop with urea, J. Phys. Chem. B 121 (2017) 3734–3746.
[13] Q.D. Pham, A. Wolde-Kidan, A. Gupta, A. Schlaich, E. Schneck, R.R. Netz, E. Sparr, Effects of urea and TMAO on lipid self-assembly under osmotic stress conditions, J. Phys. Chem. B 122 (2018) 6471–6482.
[14] D. Paschek, A.E. García, Reversible temperature and pressure denaturation of a protein fragment: a replica exchange molecular dynamics simulation study, Phys. Rev. Lett. 93 (2004) 10–13.
[15] M.R. Shirts, J.W. Pitera, W.C. Swope, V.S. Pande, Extremely precise free energy calculations of amino acid side chain analogs: comparison of common molecular mechanics force fields for proteins, J. Chem. Phys. 119 (2003) 5740–5761.
[16] D. Marx, J. Hutter, Ab Initio Molecular Dynamics - Basic Theory and Advanced Methods, Cambridge University Press, Cambridge, 2009.
[17] T. Kloss, J. Heil, S.M. Kast, Quantum chemistry in solution by combining 3D integral equation theory with a cluster embedding approach, J. Phys. Chem. B 112 (2008) 4337–4343.
[18] C. Hölzl, P. Kibies, S. Imoto, R. Frach, S. Suladze, R. Winter, D. Marx, D. Horinek, S.M. Kast, Design principles for high-pressure force fields: aqueous TMAO solutions from ambient to kilobar pressures, J. Chem. Phys. 144 (2016) 144104.
[19] J.M. Wang, R.M. Wolf, J.W. Caldwell, P.A. Kollman, D.A. Case, Development and testing of a general amber force field, J. Comput. Chem. 25 (2004) 1157–1174.
[20] S. Weerasinghe, P.E. Smith, A Kirkwood-Buff derived force field for mixtures of urea and water, J. Phys. Chem. B 107 (2003) 3891–3898.
[21] E.M. Duffy, D.L. Severance, W.L. Jorgensen, Urea: potential functions, log P, and free energy of hydration, Isr. J. Chem. 33 (1993) 323–330.
[22] D. Horinek, R.R. Netz, Can simulations quantitatively predict peptide transfer free energies to urea solutions? Thermodynamic concepts and force field limitations, J. Phys. Chem. A 115 (2011) 6125–6136.
[23] M. Knierbein, C. Held, C. Hölzl, D. Horinek, M. Paulus, S. Sadowski, C. Sternemann, J. Nase, Density variations of TMAO solutions in the kilobar range: experiments, PC-SAFT predictions, and molecular dynamics simulations, Biophys. Chem. 253 (2019) 106222.
[24] C. Caleman, P.J. van Maaren, M. Hong, J.S. Hub, L.T. Costa, D. van der Spoel, Force field benchmark of organic liquids: density, enthalpy of vaporization, heat capacities, surface tension, isothermal compressibility, volumetric expansion coefficient, and dielectric constant, J. Chem. Theory Comput. 8 (2012) 61–74.
[25] K.M. Kast, J. Brickmann, S.M. Kast, R.S. Berry, Binary phases of aliphatic N-oxides and water: force field development and molecular dynamics simulation, J. Phys. Chem. A 107 (2003) 5342–5351.
[26] F. Wirkert, C. Hölzl, M. Paulus, P. Salmen, M. Tolan, D. Horinek, J. Nase, The hydrophobic gap at high hydrostatic pressures, Angew. Chem. Int. Ed. 56 (2017) 12958–12961.
[27] L. Knake, G. Schwaab, K. Kartaschew, M. Havenith, Solvation dynamics of trimethylamine N-oxide in aqueous solution probed by terahertz spectroscopy, J. Phys. Chem. B 119 (2015) 13842–13851.
[28] X. Ji, C. Held, Modeling the density of ionic liquids with ePC-SAFT, Fluid Phase Equilib. 410 (2016) 9–22.
[29] C. Held, G. Sadowski, Compatible solutes: thermodynamic properties relevant for effective protection against osmotic stress, Fluid Phase Equilib. 407 (2016) 224–235.
[30] Y. Sun, G. Shen, C. Held, X. Feng, X. Lu, X. Ji, Modeling viscosity of ionic liquids with electrolyte perturbed-chain statistical associating fluid theory and free volume theory, Ind. Eng. Chem. Res. 57 (2018) 8784–8801.
[31] G. Shen, C. Held, X. Lu, X. Ji, Modelling interfacial properties of ionic liquids with ePC-SAFT combined with density gradient theory, Mol. Phys. 114 (2016) 2492–2499.
[32] G. Shen, C. Held, X. Lu, X. Ji, Modeling thermodynamic derivative properties of ionic liquids with ePC-SAFT, Fluid Phase Equilib. 405 (2015) 73–82.
[33] F.T.J. Gucker, F.W. Gage, C.E. Moser, The densities of aqueous solutions of urea at 25 and 30° and the apparent molal volume of urea, J. Am. Chem. Soc. 60 (1938) 2582–2588.
[34] E.P. Egan, B.B. Luff, Heat of solution, heat capacity, and density of aqueous urea solutions at 25°C, J. Chem. Eng. Data 11 (1966) 192–194.
[35] K.S. Pitzer, J.C. Peiper, R.H. Busey, Thermodynamic properties of aqueous sodium chloride solutions, J. Phys. Chem. Ref. Data 13 (1984) 1–102.
[36] Y. Tanaka, T. Yamamoto, Y. Satomi, H. Kubota, T. Makita, Specific volume and viscosity of ethanol-water mixtures under high pressure, Rev. Phys. Chem. Jpn. 47 (1977).
[37] X. Ji, C. Held, G. Sadowski, Modeling imidazolium-based ionic liquids with ePC-SAFT, Fluid Phase Equilib. 335 (2012) 64–73.
[38] C. Held, T. Neuhaus, G. Sadowski, Compatible solutes: thermodynamic properties and biological impact of ectoines and prolines, Biophys. Chem. 152 (2010) 28–39.
[39] L.F. Cameretti, G. Sadowski, Modeling of aqueous amino acid and polypeptide solutions with PC-SAFT, Chem. Eng. Process. Process Intensif. 47 (2008) 1018–1025.
[40] G. Watson, T. Lafitte, C.K. Zéberg-Mikkelsen, A. Baylaucq, D. Bessieres, C. Boned, Volumetric and derivative properties under pressure for the system 1-propanol + toluene: a discussion of PC-SAFT and SAFT-VR, Fluid Phase Equilib. 247 (2006) 121–134.
[41] J. Gross, G. Sadowski, Perturbed-chain SAFT: an equation of state based on a perturbation theory for chain molecules, Ind. Eng. Chem. Res. 40 (2001) 1244–1260.
[42] J. Gross, G. Sadowski, Application of the perturbed-chain SAFT equation of state to associating systems, Ind. Eng. Chem. Res. 41 (2002) 5510–5515.
[43] K. Suzuki, S. Onishi, T. Koide, S. Seki, Vapor pressures of molecular crystals. XI. Vapor pressures of crystalline urea and diformylhydrazine. Energies of hydrogen bonds in these crystals, Bull. Chem. Soc. Jpn. 29 (1956) 127–131.
[44] H.G.M.D. Wit, J.C.V. Miltenburg, C.G.D. Kruif, Thermodynamic properties of molecular organic crystals containing nitrogen, oxygen, and sulphur 1. Vapour pressures and enthalpies of sublimation, J. Chem. Thermodyn. 15 (1983) 651–663.
[45] V.N. Emel'yanenko, G.J. Kabo, S.P. Verevkin, Measurement and prediction of

thermochemical properties: improved increments for the estimation of enthalpies of sublimation and standard enthalpies of formation of alkyl derivatives of urea, J. Chem. Eng. Data 51 (2006) 79–87.
[46] S. Petitgirard, W. Malfait, R. Sinmyo, I. Kupenko, L. Hennet, D. Harries, T. Dane, M. Burghammer, D. Rubie, Fate of MgSiO3 melts at core-mantle boundary conditions, Proc. Natl. Acad. Sci. U. S. A. 112 (2015) 14186–14190.
[47] S. Petitgirard, W. Malfait, B. Journaux, I. Collings, E. Jennings, I. Blanchard, I. Kantor, A. Kurnosov, M. Cotte, T. Dane, et al., SiO2 glass density to lower-mantle pressures, Phys. Rev. Lett. 119 (2017) 215701.
[48] F.J. Wirkert, M. Paulus, J. Nase, J. Möller, S. Kujawski, C. Sternemann, M. Tolan, X-ray reflectivity measurements of liquid/solid interfaces under high hydrostatic pressure conditions, J. Synchrotron Radiat. 21 (2014) 76–81.
[49] E.W. Lemmon, M.O. McLinden, D.G. Friend, Thermophysical Properties of Fluid Systems in NIST Chemistry WebBook, NIST Standard Reference Database Number 69, in: P.J. Linstrom, W.G. Mallard (Eds.), National Institute of Standards and Technology, Gaithersburg MD, 2018, p. 20899 (retrieved December 5, 2018).
[50] M.J. Berger, J.H. Hubbell, S.M. Seltzer, J. Chang, J.S. Coursey, R. Sukumar, D.S. Zucker, K. Olsen, XCOM: Photon Cross Section Database (version 1.5). [Online], National Institute of Standards and Technology, Gaithersburg, MD, 2010 Available: http://physics.nist.gov/xcom (2019, September 3).
[51] D. Lützenkirchen-Hecht, R. Wagner, U. Haake, A. Watenphul, R. Frahm, The materials science X-ray beamline BL8 at the DELTA storage ring, J. Synchrotron Radiat. 16 (2009) 264–272.
[52] J. Hutter, M. Iannuzzi, F. Schiffmann, J. VandeVondele, CP2K: atomistic simulations of condensed matter systems, Wiley Interdisc. Rev. Comput. Mol. Sci. 4 (2013) 15–25.
[53] J. VandeVondele, M. Krack, F. Mohamed, M. Parrinello, T. Chassaing, J. Hutter, Quickstep: fast and accurate density functional calculations using a mixed Gaussian and plane waves approach, Comput. Phys. Commun. 167 (2005) 103–128.
[54] B. Hammer, L.B. Hansen, J.K. Nørskov, Improved adsorption energetics within density-functional theory using revised Perdew-Burke-Ernzerhof functionals, Phys. Rev. B 59 (1999) 7413–7421.
[55] S. Lehtola, C. Steigemann, M.J. Oliveira, M.A. Marques, Recent developments in libxc – a comprehensive library of functionals for density functional theory, SoftwareX 7 (2018) 1–5.
[56] S. Grimme, J. Antony, S. Ehrlich, H. Krieg, A consistent and accurate ab initio parametrization of density functional dispersion correction (DFT-D) for the 94 elements H-Pu, J. Chem. Phys. 132 (2010) 154104.
[57] K. Tonigold, A. Groß, Dispersive interactions in water bilayers at metallic surfaces: a comparison of the PBE and RPBE functional including semiempirical dispersion corrections, J. Comput. Chem. 33 (2012) 695–701.
[58] T. Morawietz, J. Behler, A density-functional theory-based neural network potential for water clusters including van der Waals corrections, J. Phys. Chem. A 117 (2013) 7356–7366.
[59] K. Forster-Tonigold, A. Groß, Dispersion corrected RPBE studies of liquid water, J. Chem. Phys. 141 (2014) 064501.
[60] S. Imoto, H. Forbert, D. Marx, Water structure and solvation of osmolytes at high hydrostatic pressure: pure water and TMAO solutions at 10 kbar versus 1 bar, Phys. Chem. Chem. Phys. 17 (2015) 24224–24237.
[61] T. Morawietz, A. Singraber, C. Dellago, J. Behler, How van der Waals interactions determine the unique properties of water, Proc. Natl. Acad. Sci. U. S. A. 113 (2016) 8368–8373.
[62] S. Imoto, P. Kibies, C. Rosin, R. Winter, S.M. Kast, D. Marx, Toward extreme biophysics: deciphering the infrared response of biomolecular solutions at high pressures, Angew. Chem. Int. Ed. 55 (2016) 9534–9538.
[63] M. Hellström, J. Behler, Concentration-dependent proton transfer mechanisms in aqueous NaOH solutions: from acceptor-driven to donor-driven and back, J. Phys. Chem. Lett. 7 (2016) 3302–3306.
[64] S. Sakong, K. Forster-Tonigold, A. Groß, The structure of water at a Pt (111) electrode and the potential of zero charge studied from first principles, J. Chem. Phys. 144 (2016) 194701.
[65] P. Schienbein, D. Marx, Liquid–vapor phase diagram of RPBE-D3 water: electronic properties along the coexistence curve and in the supercritical phase, J. Phys. Chem. B 122 (2018) 3318–3329.
[66] P.K. Gupta, J. Daru, P. Schienbein, D. Marx, Terahertz spectra of microsolvated ions: do they reveal bulk solvation properties? J. Phys. Chem. Lett. 10 (2019) 393–398.
[67] J. Daru, P.K. Gupta, D. Marx, Restricting solvation to two dimensions: soft-landing of microsolvated ions on inert surfaces, J. Phys. Chem. Lett. 10 (2019) 831–835.
[68] S. Imoto, D. Marx, Pressure response of the THz spectrum of bulk liquid water revealed by intermolecular instantaneous normal mode analysis, J. Chem. Phys. 150 (2019) 084502.
[69] G. Lippert, J. Hutter, M. Parrinello, A hybrid Gaussian and plane wave density functional scheme, Mol. Phys. 92 (1997) 477–488.
[70] J. VandeVondele, J. Hutter, Gaussian basis sets for accurate calculations on molecular systems in gas and condensed phases, J. Chem. Phys. 127 (2007) 114105.
[71] S. Goedecker, M. Teter, J. Hutter, Separable dual-space Gaussian pseudopotentials, Phys. Rev. B 54 (1996) 1703–1710.
[72] C. Hartwigsen, S. Goedecker, J. Hutter, Relativistic separable dual-space Gaussian pseudopotentials from H to Rn, Phys. Rev. B 58 (1998) 3641–3662.
[73] G.J. Martyna, M.L. Klein, M. Tuckerman, Nosé–Hoover chains: the canonical ensemble via continuous dynamics, J. Chem. Phys. 97 (1992) 2635–2643.
[74] M.J. Frisch, G.W. Trucks, H.B. Schlegel, G.E. Scuseria, M.A. Robb, J.R. Cheeseman, J.A. Montgomery Jr., T. Vreven, K.N. Kudin, J.C. Burant, et al., Gaussian 03, Revision E.01, Gaussian Inc., Wallingford CT, 2004.
[75] B. Hess, C. Kutzner, D. van der Spoel, E. Lindahl, GROMACS 4: algorithms for highly efficient, load-balanced, and scalable molecular simulation, J. Chem. Theory Comput. 4 (2008) 435–447.
[76] M. Brehm, B. Kirchner, TRAVIS – a free analyzer and visualizer for monte carlo and molecular dynamics trajectories, J. Chem. Inf. Model. 51 (2011) 2007–2023.
[77] W. Humphrey, A. Dalke, K. Schulten, VMD – visual molecular dynamics, J. Mol. Graph. 14 (1996) 33–38.
[78] U. Essmann, L. Perera, M.L. Berkowitz, T. Darden, H. Lee, L.G. Pedersen, A smooth particle mesh Ewald method, J. Chem. Phys. 103 (1995) 8577.
[79] S. Miyamoto, P. Kollman, SETTLE: an analytical version of the SHAKE and RATTLE algorithm for rigid water models, J. Comput. Chem. 13 (1992) 952–962.
[80] B. Hess, P-LINCS: a parallel linear constraint solver for molecular simulation, J. Chem. Theory Comput. 4 (2008) 116–122.
[81] G. Bussi, D. Donadio, M. Parrinello, Canonical sampling through velocity rescaling, J. Chem. Phys. 126 (2007) 014101.
[82] H.J.C. Berendsen, J.P.M. Postma, W.F. van Gunsteren, A. DiNola, J.R. Haak, Molecular dynamics with coupling to an external bath, J. Chem. Phys. 81 (1984) 3684.
[83] M. Parrinello, A. Rahman, Polymorphic transitions in single crystals: a new molecular dynamics method, J. Appl. Phys. 52 (1981) 7182.
[84] J.L.F. Abascal, C. Vega, A general purpose model for the condensed phases of water: TIP4P/2005, J. Chem. Phys. 123 (2005) 234505.
[85] H.J.C. Berendsen, J.R. Grigera, T.P. Straatsma, The missing term in effective pair potentials, J. Phys. Chem. 91 (1987) 6269–6271.
[86] R. Storn, K. Price, Differential evolution – a simple and efficient heuristic for global optimization over continuous spaces, J. Glob. Optim. 11 (1997) 341–359.
[87] J.G. Kirkwood, F.P. Buff, The statistical mechanical theory of solutions. I, J. Chem. Phys. 19 (1951) 774.
[88] P. Ganguly, N.F.A. van der Vegt, Convergence of sampling Kirkwood-Buff integrals of aqueous solutions with molecular dynamics simulations, J. Chem. Theory Comput. 9 (2013) 1347–1355.
[89] R. Cortes-Huerto, K. Kremer, R. Potestio, Communication: Kirkwood-Buff integrals in the thermodynamic limit from small-sized molecular dynamics simulations, J. Chem. Phys. 145 (2016) 141103.
[90] P. Krüger, S.K. Schnell, D. Bedeaux, S. Kjelstrup, T.J.H. Vlugt, J.M. Simon, Kirkwood-Buff integrals for finite volumes, J. Phys. Chem. Lett. 4 (2013) 235–238.
[91] N. Dawass, P. Krüger, S.K. Schnell, D. Bedeaux, S. Kjelstrup, J.M. Simon, T.J.H. Vlugt, Finite-size effects of Kirkwood–Buff integrals from molecular simulations, Mol. Simul. 44 (2018) 599–612.
[92] W.B. Floriano, M.A.C. Nascimento, Dielectric constant and density of water as a function of pressure at constant temperature, Braz. J. Phys. 34 (2004) 38–41.
[93] C. Held, J. Brinkmann, A.-D. Schröder, M.I. Yagofarov, S.P. Verevkin, Solubility predictions of acetanilide derivatives in water: combining thermochemistry and thermodynamic modeling, Fluid Phase Equilib. 455 (2018) 43–53.
[94] K.V. Zherikova, A.A. Svetlov, M.A. Varfolomeev, S.P. Verevkin, C. Held, Thermochemistry of halogenobenzoic acids as an access to PC-SAFT solubility modeling, Fluid Phase Equilib. 409 (2016) 399–407.
[95] V.N. Emel'yanenko, D.H. Zaitsau, E. Shoifet, F. Meurer, S.P. Verevkin, C. Schick, C. Held, Benchmark thermochemistry for biologically relevant adenine and cytosine. A combined experimental and theoretical study, J. Phys. Chem. A 119 (2015) 9680–9691.
[96] W.H. Johnson, Enthalpies of combustion and formation of acetanilide and urea, J. Res. Natl. Bur. Stand. 79 (1975) 487–491.
[97] J. Wyman, Dielectric constants: ethanol-diethyl ether and urea-water solutions between 0 and 50°, J. Am. Chem. Soc. 55 (1933) 4116–4121.
[98] H. Endo, The adiabatic compressibility of nonelectrolyte aqueous solutions in relation to the structures of water and solutions, Bull. Chem. Soc. Jpn. 46 (1973) 1106–1111.
[99] C. Vega, J.L. Abascal, Simulating water with rigid non-polarizable models: a general perspective, Phys. Chem. Chem. Phys. 13 (2011) 19663–19688.
[100] M. Neumann, Dipole moment fluctuation formulas in computer simulations of polar systems, Mol. Phys. 50 (1983) 841–858.
[101] G. Scatchard, W.J. Hamer, S.E. Wood, Isotonic solutions. I. The chemical potential of water in aqueous solutions of sodium chloride, potassium chloride, sulfuric acid, sucrose, urea and glycerol at 25°, J. Am. Chem. Soc. 60 (1938) 3061–3070.
[102] P.J. Dunlop, L.J. Gosting, A study of the diffusion of glycolamide in water at 25° with the Gouy interference method, J. Am. Chem. Soc. 75 (1953) 5073–5075.
[103] G.R. Medders, V. Babin, F. Paesani, Development of a "first-principles" water potential with flexible monomers. III. Liquid phase properties, J. Chem. Theory Comput. 10 (2014) 2906–2910.
[104] P. Ganguly, T. Hajari, J.E. Shea, N.F. Van Der Vegt, Mutual exclusion of urea and trimethylamine N-oxide from amino acids in mixed solvent environment, J. Phys. Chem. Lett. 6 (2015) 581–585.
[105] T. Pongratz, P. Kibies, L. Eberlein, N. Tielker, C. Hölzl, S. Imoto, M.B. Erlach, S. Kurrmann, P.H. Schummel, et al., Pressure-dependent electronic structure calculations using integral equation-based solvation models, Biophys. Chem. (2019) 106258.